Electronic Supplementary Material (ESI) for Journal of Materials Chemistry A.

Supporting Information for

Fast fabrication of self-supported porous nickel phosphide foam for efficient, durable oxygen evolution and overall water splitting

*Xiaoguang Wang, Wei Li, Dehua Xiong, and Lifeng Liu**

International Iberian Nanotechnology Laboratory (INL), Av. Mestre Jose Veiga, 4715-330 Braga, Portugal

*Email: lifeng.liu@inl.int (L.L.)

Estimation of the energy efficiency of water electrolyzers:

Water electrolysis involves the hydrogen evolution reaction (HER) on cathode and the oxygen evolution reaction (OER) on anode. The minimal cell voltage for water electrolysis in an open system, E^0_{cell}, is given by the following equation under standard conditions (25 °C, 1 atm, P, T constant):

$$E^0_{cell} = -\frac{\Delta G^0}{nF} \quad (1)$$

$$\text{or } \Delta G^0 = -nFE^0_{cell} \quad (2)$$

Where ΔG^0 is the change in the Gibbs free energy under standard conditions and n is the number of electrons transferred.

$$\Delta G^0 = \Delta H^0 - TR\Delta n - T\Delta S^0 \quad (3)$$

For the electrolysis of water, the standard reaction enthalpy is ΔH^0 = 285.8 kJ mol^{-1}, Δn = 1.5, ΔS^0 (H_2) = 130.6 J mol^{-1}, ΔS^0(O_2) = 205.1 J mol^{-1}, ΔS^0(H_2O) (l) = 70 J mol^{-1} K^{-1}, ΔS^0_{tot} = 130.6 + ½ 205.1 – 70 = 163.14 J mol^{-1} K^{-1}, and ΔG^0 = 237.2 kJ mol^{-1}. So the minimum cell voltage for an open cell is E^0_{cell} = - $\Delta G^0/nF$ = 1.23 V, according to the equation (1).[S1]

The maximum possible efficiency of an ideal open electrochemical cell is defined by the following equation:

$$\varepsilon_{max} = \frac{\Delta H^0}{\Delta G} = -\frac{\Delta H^0}{nFE_{cell}} \quad (4)$$

where E_{cell} is the cell voltage to drive water splitting at the current of I:

$$E_{cell} = E^0_{cell} + IR + \Sigma\eta \quad (5)$$

Where R is the total ohmic series resistance in the cell including resistance of external circuit, electrolyte, electrodes, and membrane materials (if any); $\Sigma\eta$ is the sum of overpotentials including the activation overpotential at the two electrodes and the concentration overpotential.

The splitting of water by electrolysis is an endothermic reaction with the enthalpy change defined as follows:

$$\Delta H^0 = \Delta G^0 + T\Delta S = - nFE^0_{cell} + T\Delta S \quad (6)$$

Where ΔG^0 supplies energy in the form of electricity and the rest, $T\Delta S$, by heat. In actual electrolysis, cell voltage is always higher than the theoretical voltage of eletrolysis, namely reversible voltage E^0_{cell} = 1.23 V, and the difference is converted into heat. When the cell voltage reaches 1.48 V, all heat generated by overpotential and ohmic loss is used by the reaction, and at this voltage there is no heat generation or absorption to and from outside of the system (i.e., ΔS = 0). Therefore, the cell voltage of 1.48 V is defined as "thermoneutral potential" where the cell does not heat or cool and all electric energy used for electrolysis is converted into heat content of evolved gas.[S1, S2] This voltage is used as the standard of 100% efficiency. Since the current efficiency is almost 100% in water electrolysis, dividing 1.48 V by practical cell voltage (E_{cell}) will thus approximately give the energy efficiency of water electrolysis:

$$\varepsilon \cong \frac{1.48\ V}{E_{cell}} \times 100\% \quad (7)$$

Supporting Movies:

Movie S1. Video showing the O_2 evolution during galvanostatic OER electrolysis in a three-electrode configuration.

http://cloud.inl.int/f/cb7f0b6104/?raw=1 (Direct download link)

Movie S2. Overall water splitting using the alkaline electrolyzers constructed with two identical porous Ni-P foam electrodes.

http://cloud.inl.int/f/eb72d7259c/?raw=1 (Direct download link)

Supporting Figures:

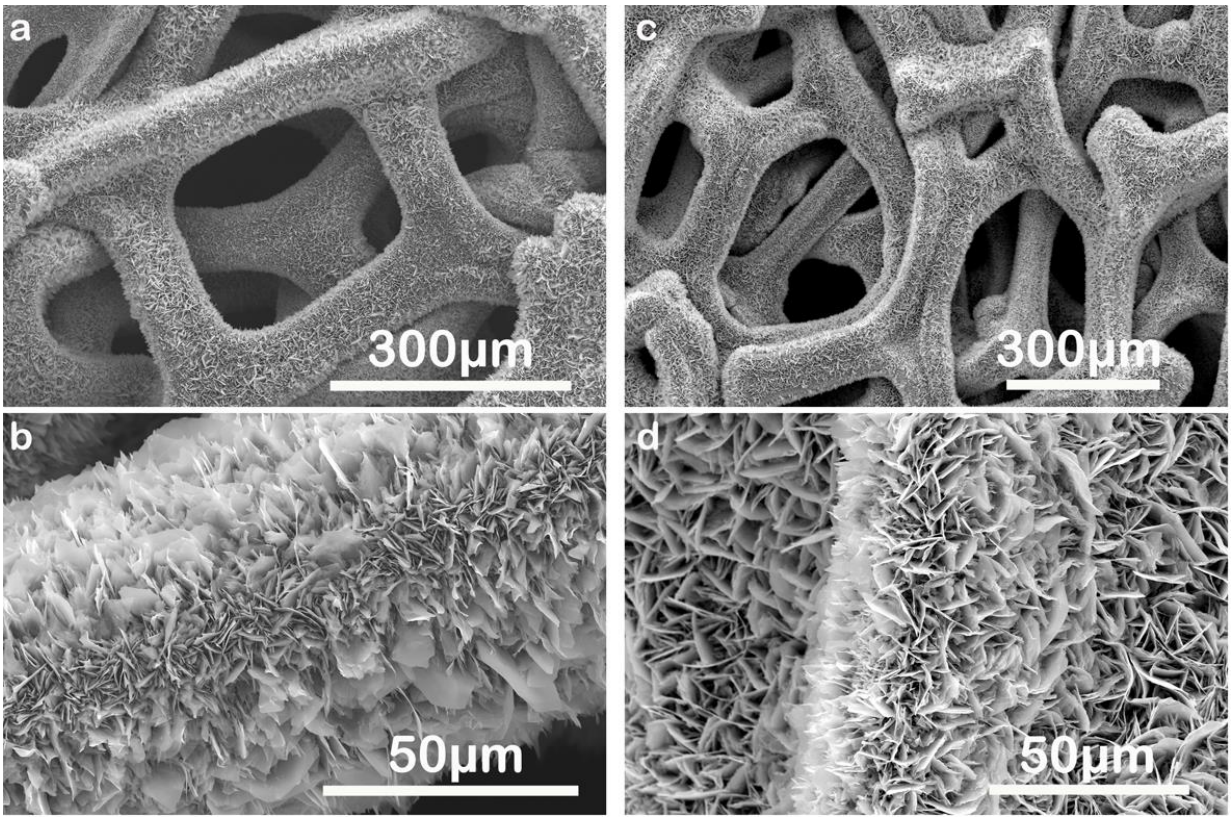

Figure S1. Morphology of the self-supported porous Ni-P foam electrodes obtained by phosphorizing Ni foam in phosphorous vapor at 500 ℃ for (a, b) 15 and (c, d) 60 min.

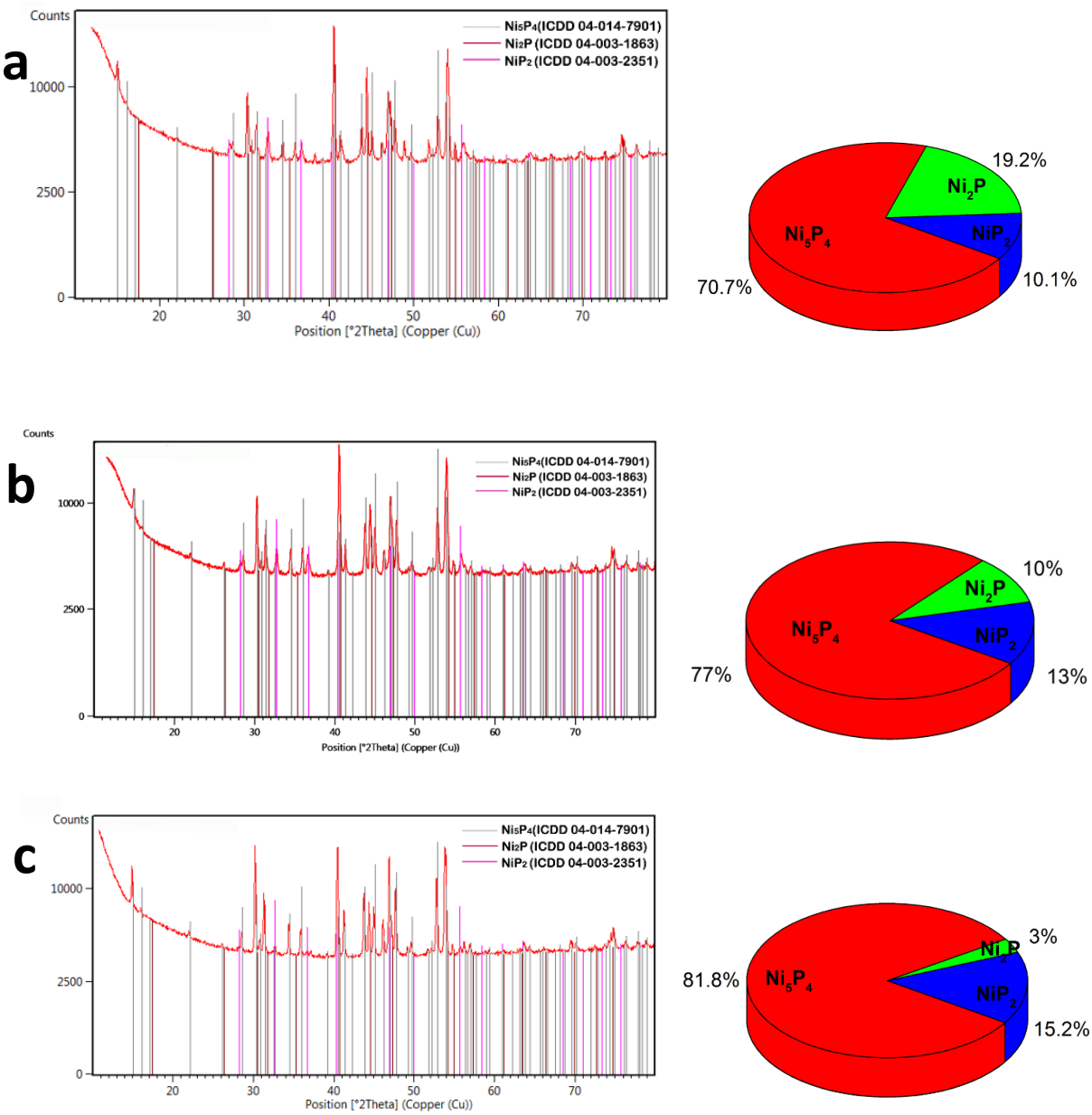

Figure S2. XRD patterns and quantitative phase composition analysis of the self-supported porous Ni-P foam electrodes obtained by phosphorizing Ni foam for (a) 15, (b) 30, and (c) 60 min. The percentage of P-rich phases (i.e., Ni_5P_4 and NiP_2) increases with the increasing phosphorization duration. No diffraction peaks from Ni was observed, indicating that the Ni foam has been completely converted into Ni-P.

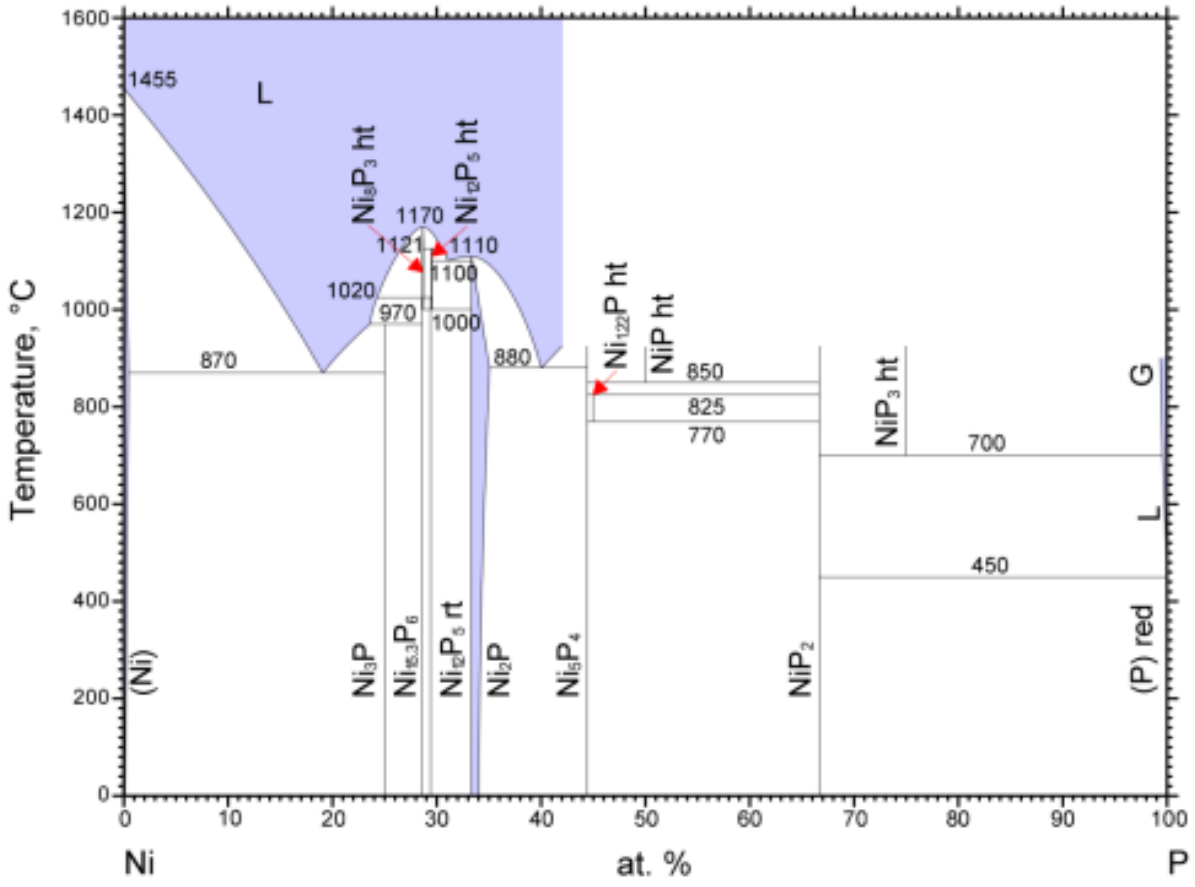

Figure S3. Ni-P phase diagram.[S3]

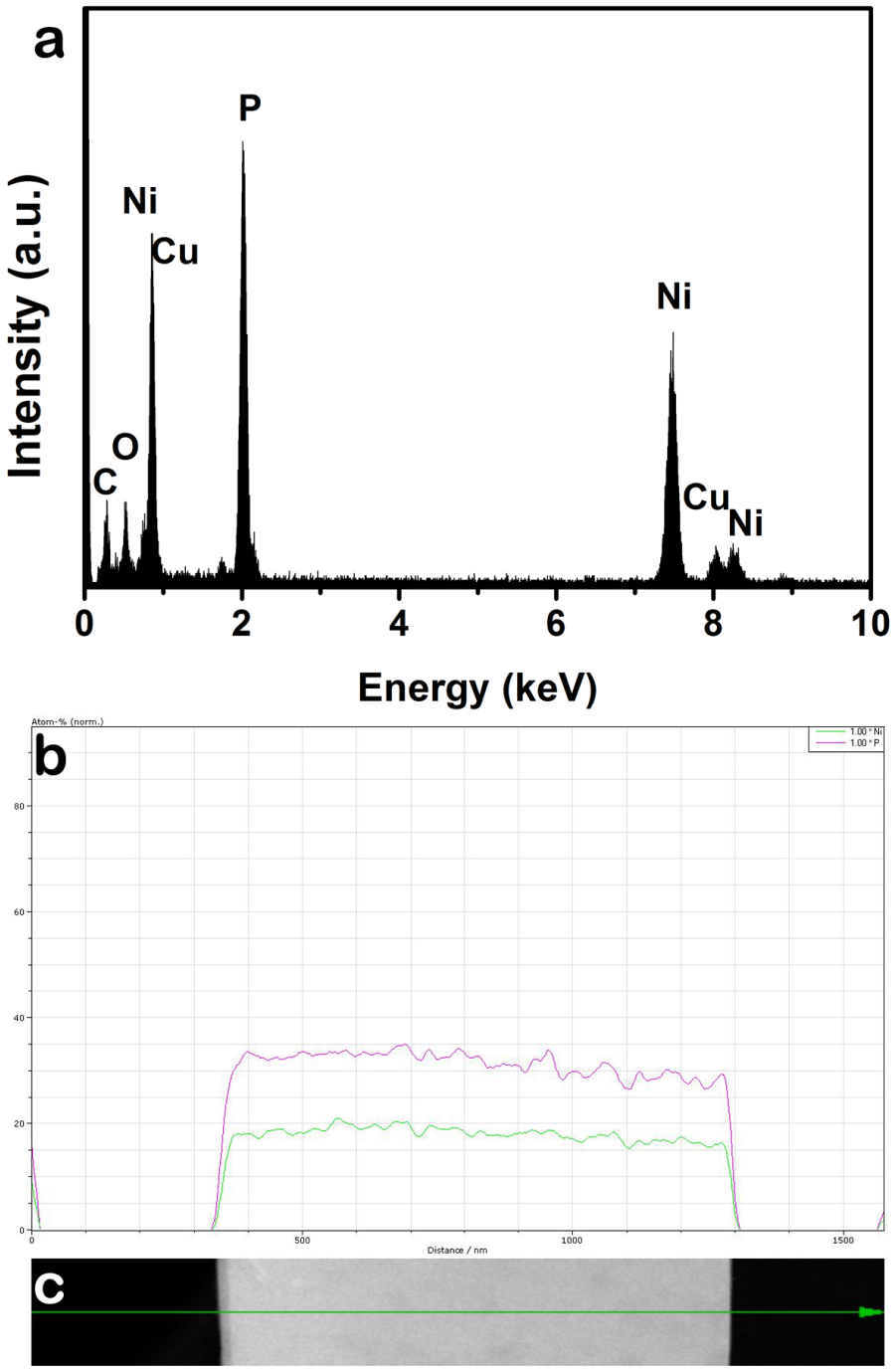

Figure S4. (a) EDX spectrum of a representative NiP_2 nanosheet; (b) STEM-EDX line scan over a NiP_2 nanosheet; (c) HAADF-STEM image of the NiP_2 nanosheet.

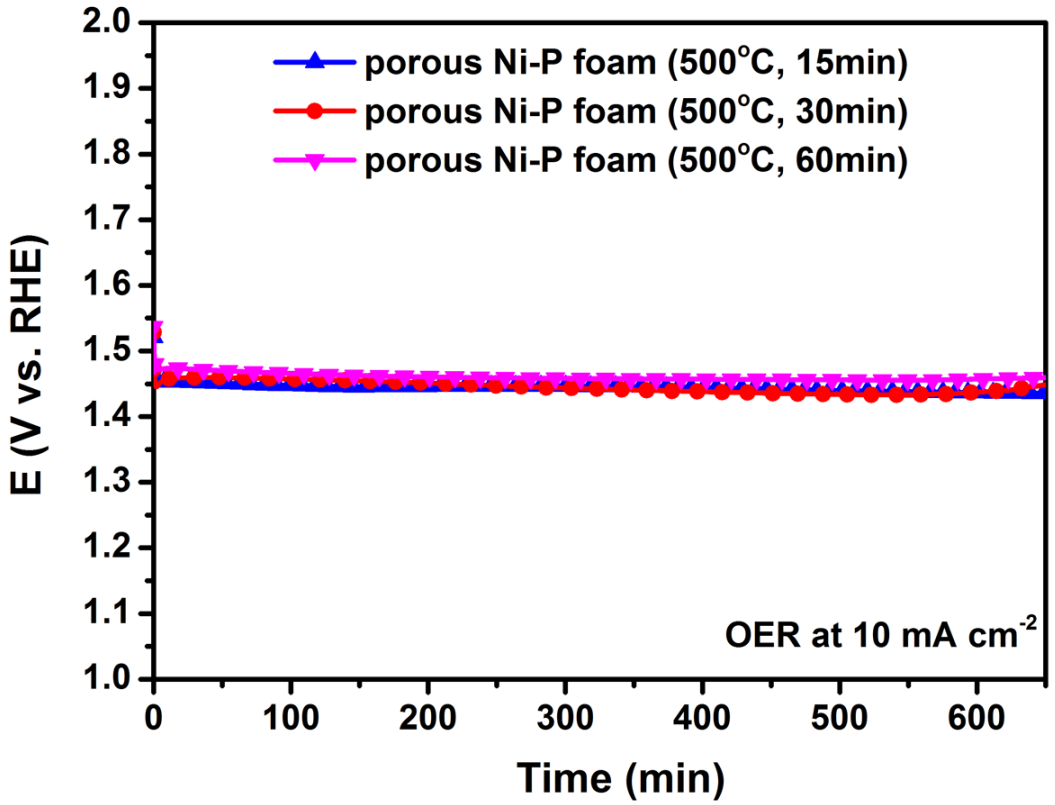

Figure S5. Galvanostatic OER electrolysis tests for self-supported porous Ni-P foam electrodes obtained by phosphorizing Ni foam at 500 °C for 15, 30, and 60 min. Current density: 10 mA cm^{-2}. Electrolyte: 1.0 M KOH. These three samples show similar electrocatalytic performance.

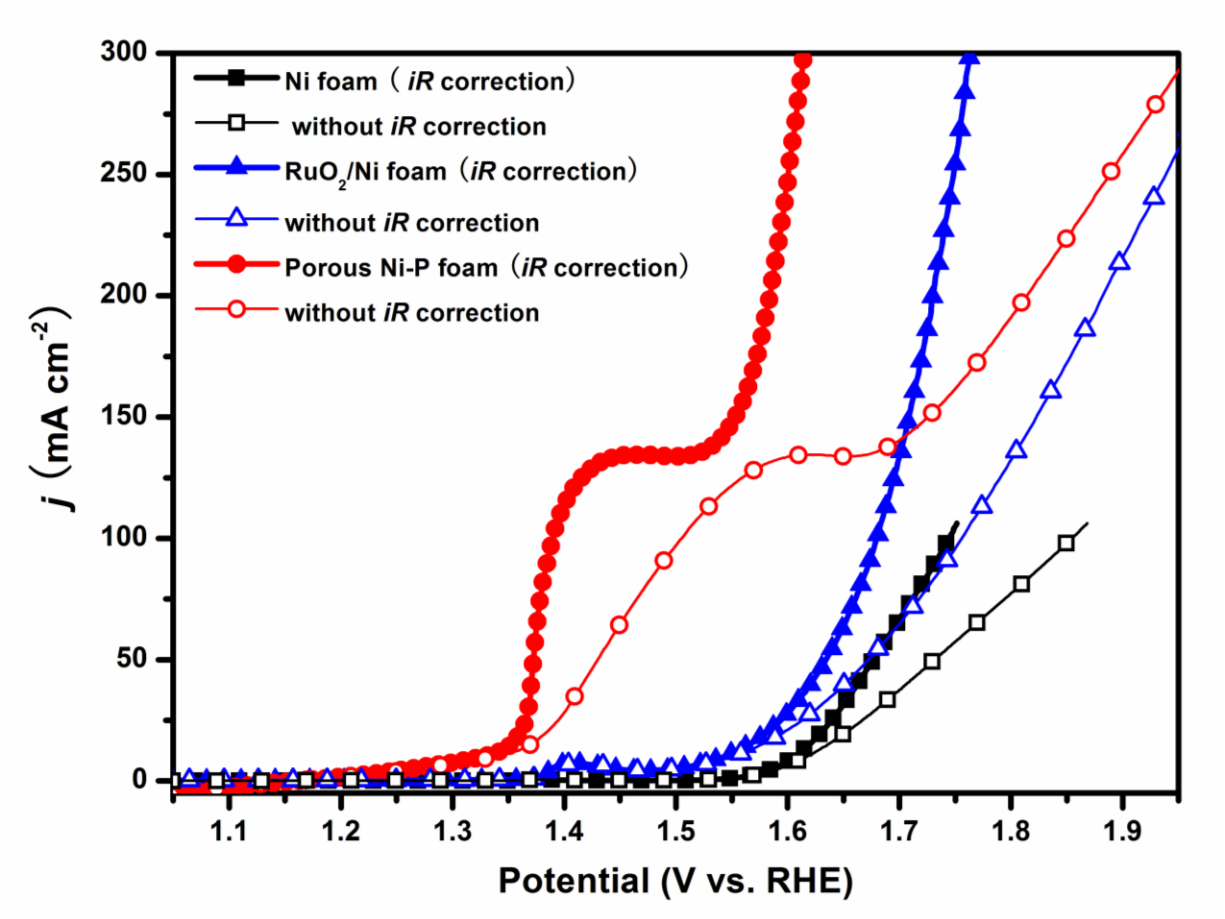

Figure S6. *iR*-corrected and non-*iR*-corrected polarization curves of a porous Ni-P foam, a RuO_2/Ni foam, and a bare Ni foam for OER in 1.0 M KOH solution. Scan rate: 5 mV s^{-1}. The equivalent series resistance (R_s) was determined to be 1.15, 0.76, and 1.10 Ω for the porous Ni-P foam, RuO_2/Ni foam, and bare Ni foam electrodes, respectively, using electrochemical impedance spectroscopy (The geometric electrode surface was ca. 1 cm^2). The *iR*-correction aims to eliminate the influence of internal resistance of electrochemical testing system on the intrinsic catalytic activity of the supported active materials, including the resistance from electrolyte, electrocatalysts themselves, catalyst/support interface, and electrical wiring. The correction can be made large at a high current density region.

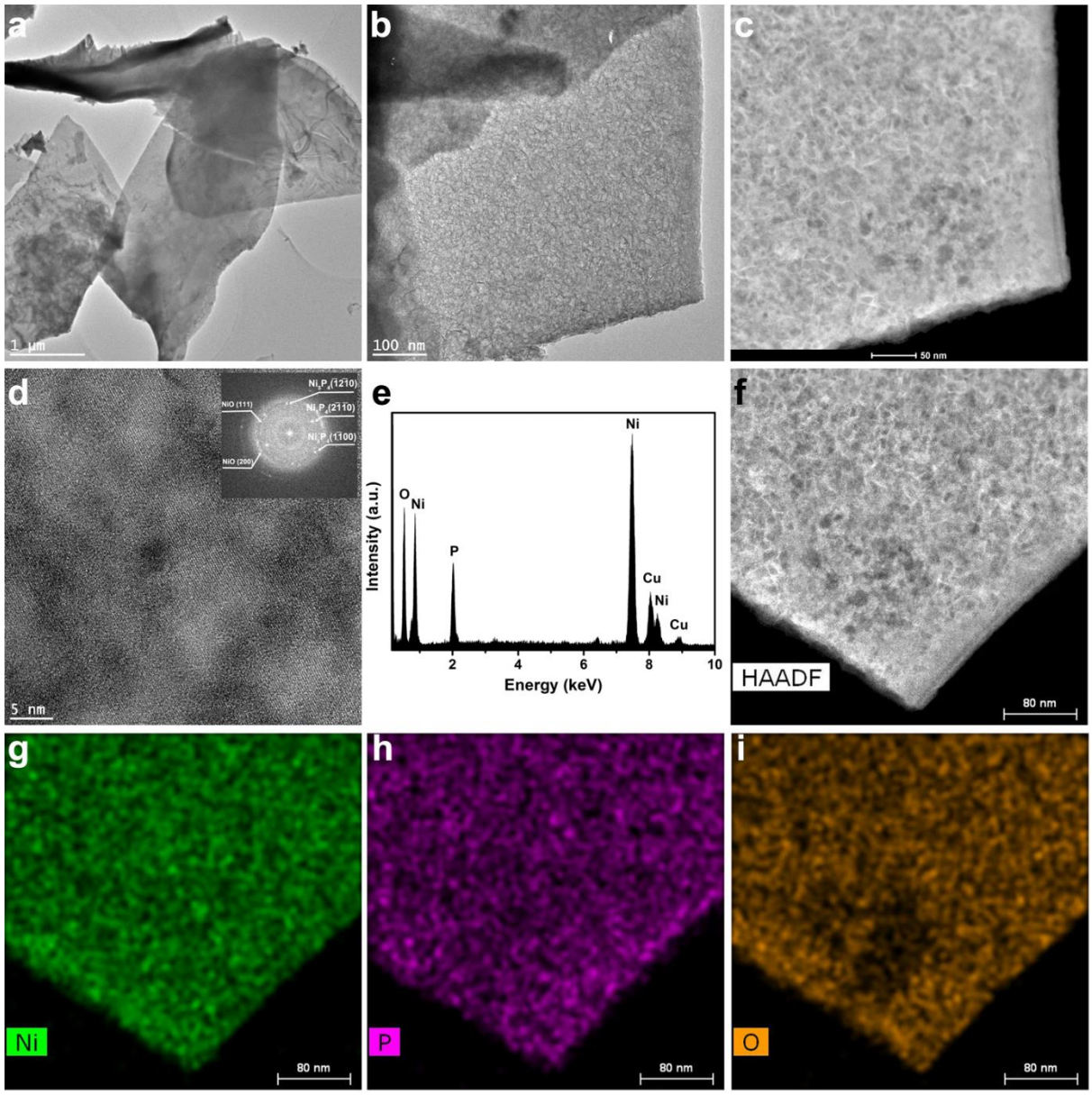

Figure S7. TEM characterization of porous Ni-P subjected to the OER catalysis at 10 mA cm^{-2} for 20 min. (a) Low- and (b) high-magnification TEM image. (c) HAADF-STEM image. (d) HRTEM image. Inset: FFT-ED pattern. (e) EDX spectrum. (f) HADDF-STEM image and elemental maps of (g) Ni, (h) P, and (i) O. Note that the NSs become rough after the OER for 20 min (b, c). However, the single-crystallinity is still retained, as evidenced by the well-defined FFT-ED pattern of Ni_5P_4 (d, inset). Nevertheless, a new phase having a poor crystallinity starts to appear which can be identified as NiO (d, inset). The presence of a large amount of oxygen is also evidenced by EDX spectrum (e) and STEM elemental mapping (i).

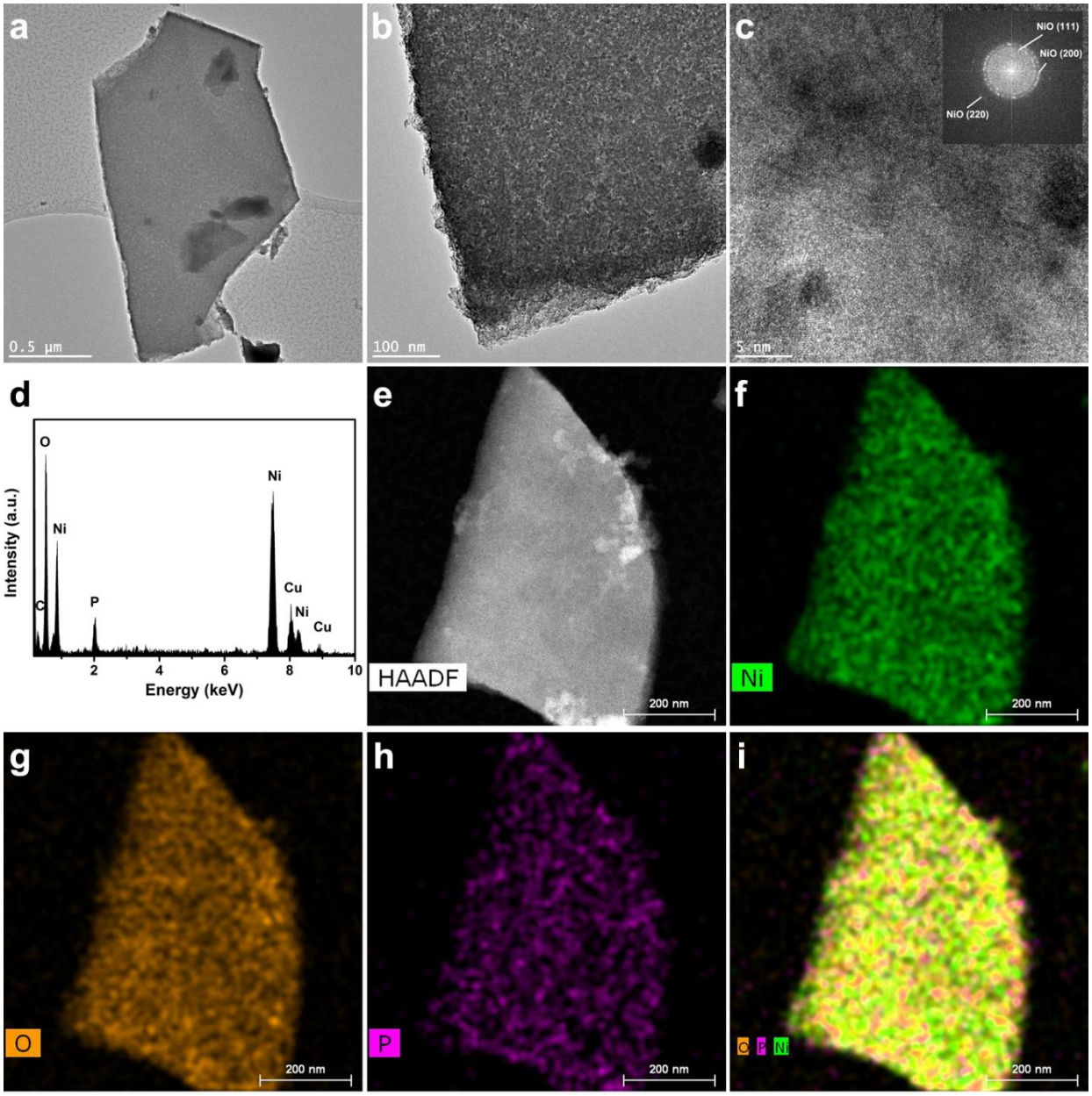

Figure S8. TEM characterization of porous Ni-P subjected to the OER catalysis at 10 mA cm^{-2} for 60 min. (a) Low- and (b) high-magnification TEM image. (c) HRTEM image. Inset: FFT-ED pattern. (d) EDX spectrum. (e) HADDF-STEM image and elemental maps of (f) Ni, (g) P, (h) O, and (i) their overlap. Note that the NSs become porous (b) and no crystallized Ni_5P_4 phase can be resolved according to FFT-ED analysis (c, inset). Instead, diffraction rings of polycrystalline NiO is clearly distinguished. The P content is further reduced and O content increased, compared to the sample subjected to OER for 20 min, as evidenced by EDX spectrum and STEM elemental mapping (d, h).

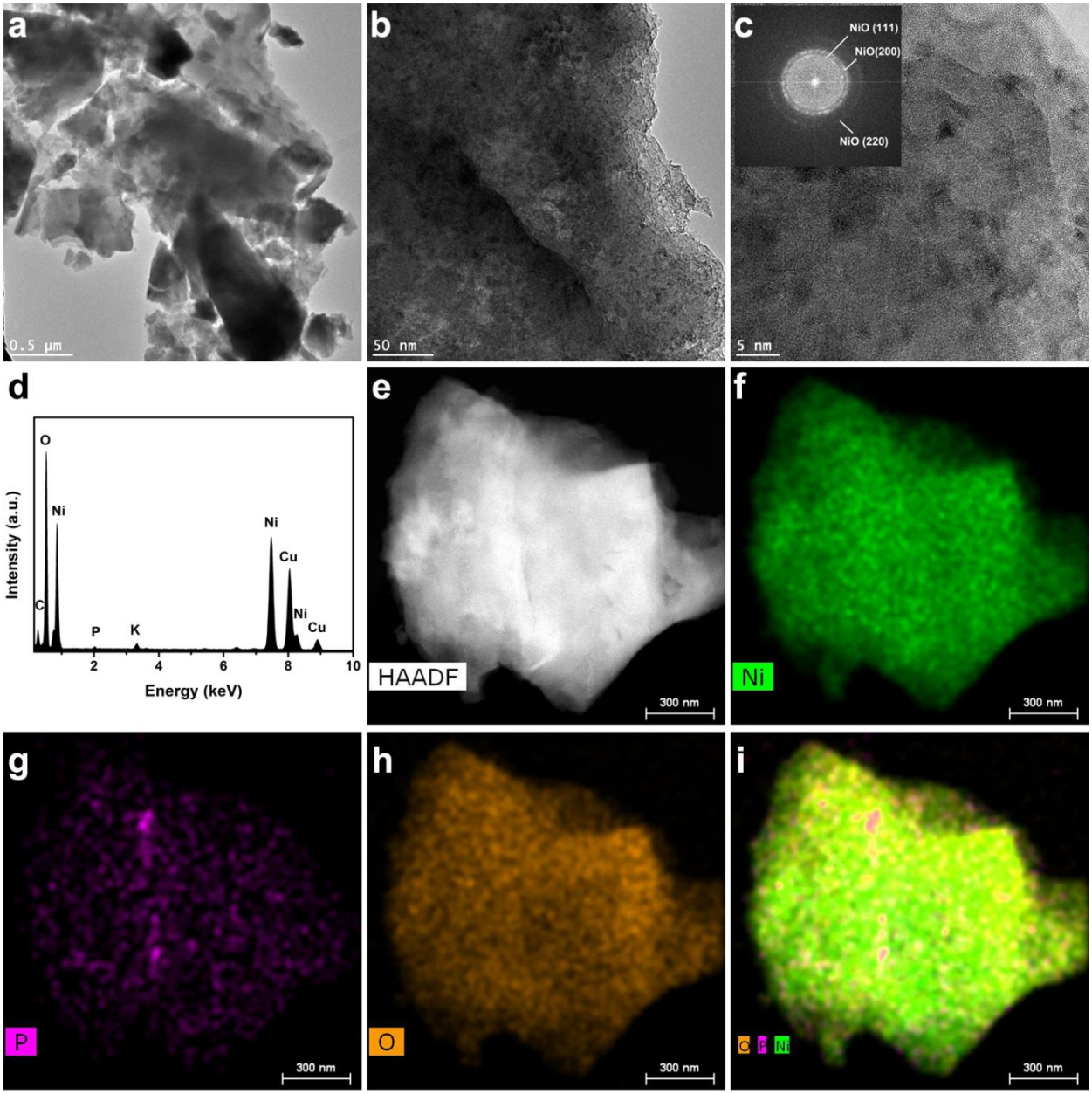

Figure S9. TEM characterization of porous Ni-P subjected to the OER catalysis at 10 mA cm^{-2} for 600 min. (a) Low- and (b) high-magnification TEM image. (c) HRTEM image. Inset: FFT-ED pattern. (d) EDX spectrum. (e) HADDF-STEM image and elemental maps of (f) Ni, (g) P, (h) O, and (i) their overlap. Note that after OER electrolysis for 600 min, the P signal becomes significantly lower according to the elemental analysis (d, g), indicating that P is virtually completely leached out.

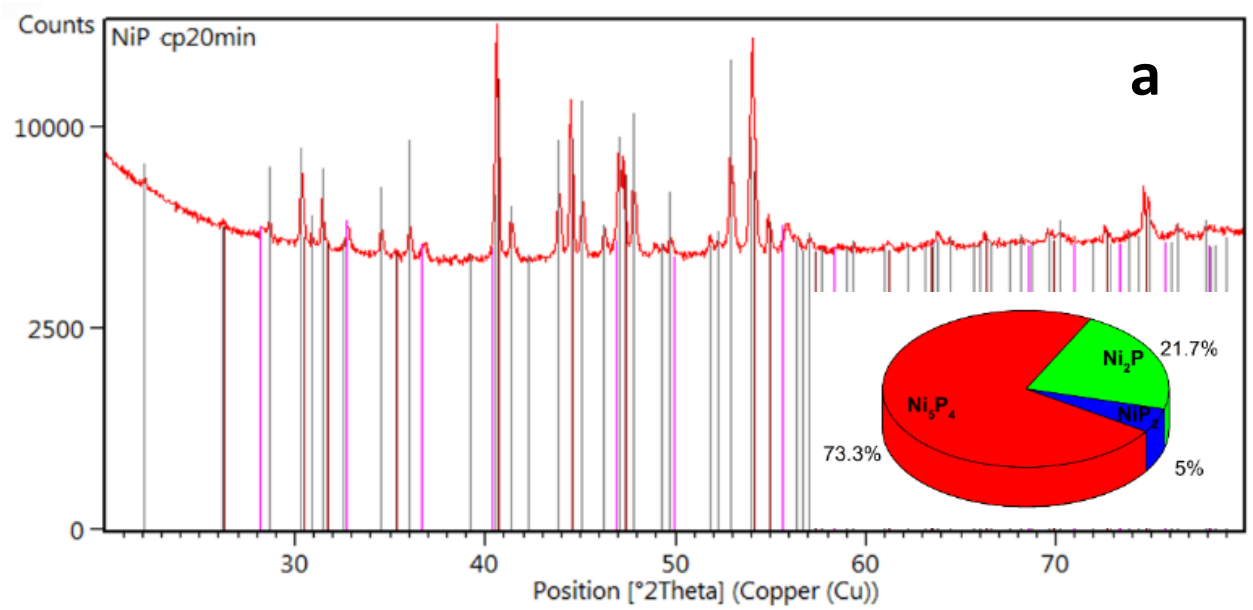
Counts
NiP cp20min
a
10000
2500
0
30
40
50
60
70
Position [°2Theta] (Copper (Cu))
Ni2P
21.7%
Ni5P4
NiP2
73.3%
5%

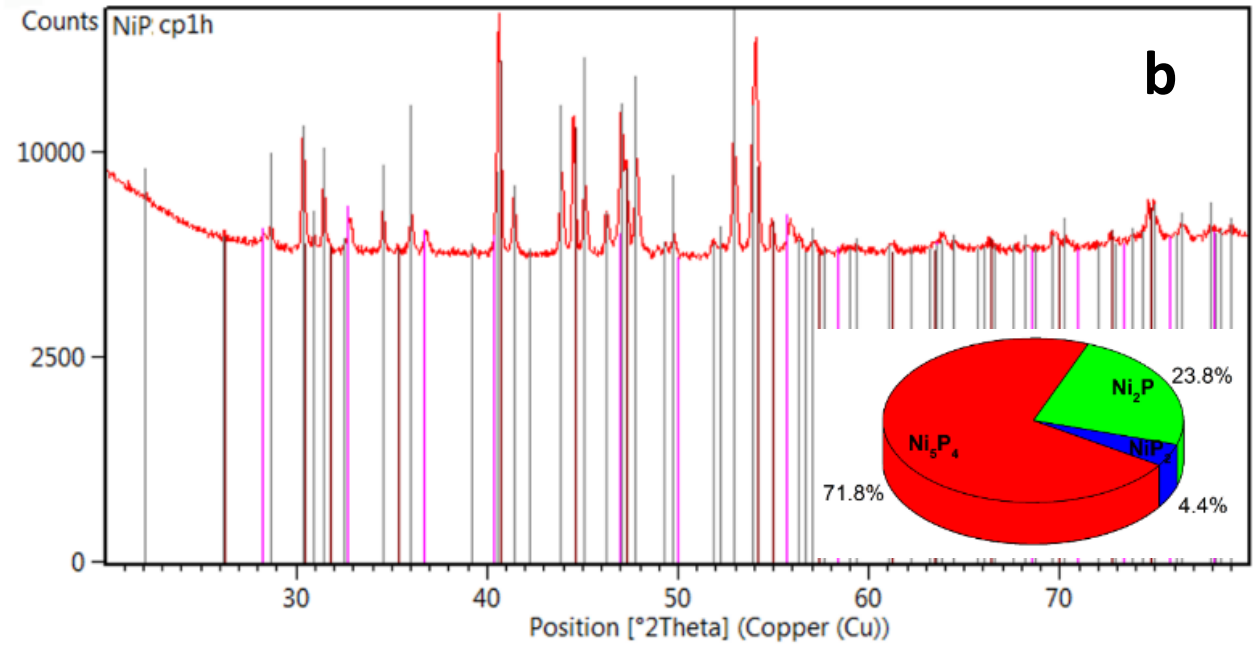
Counts
NiP cp1h
b
10000
2500
0
30
40
50
60
70
Position [°2Theta] (Copper (Cu))
Ni2P
23.8%
Ni5P4
NiP2
71.8%
4.4%

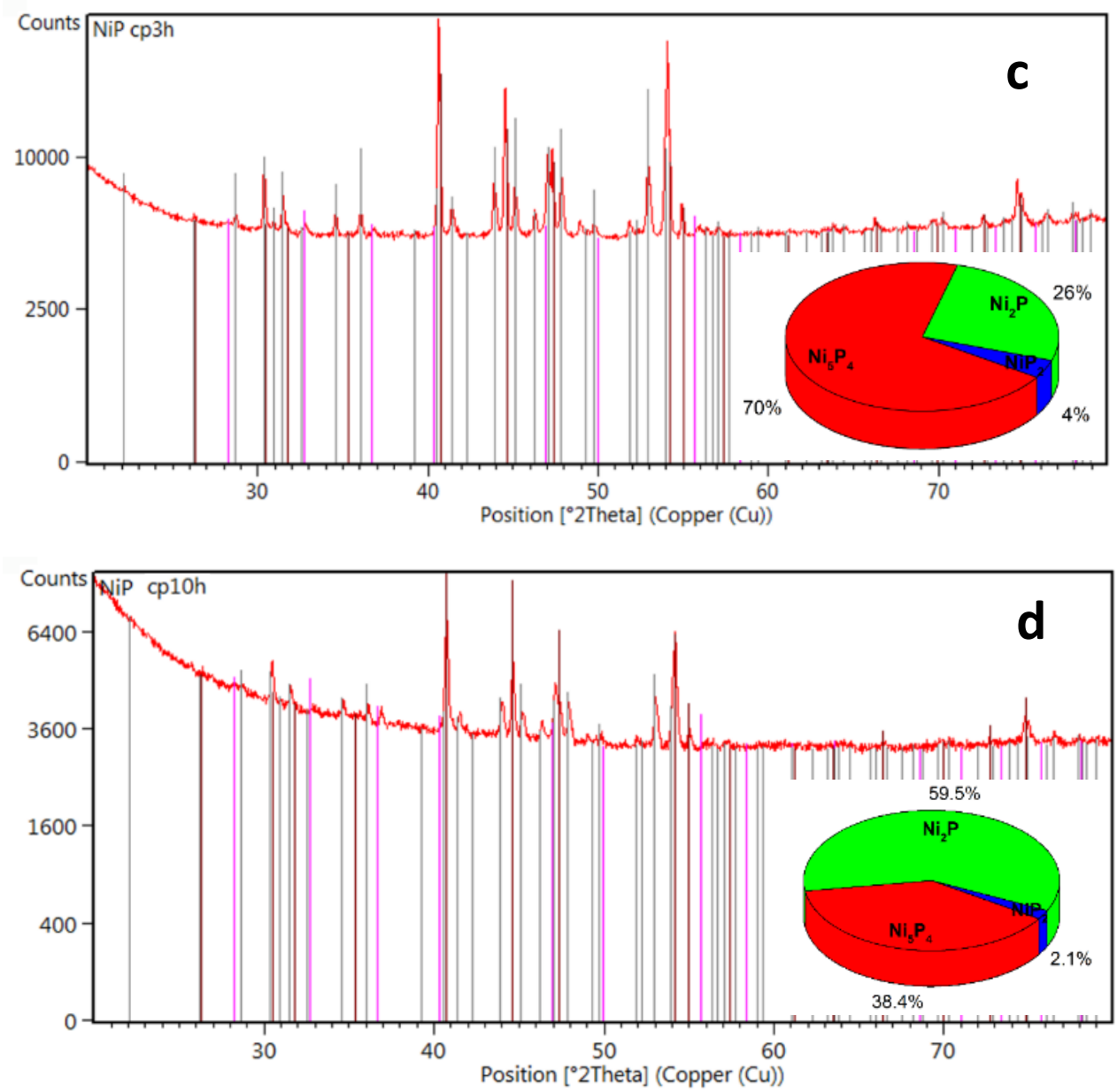

Figure S10. Quantitative phase composition analysis of the porous Ni-P foam electrodes subjected to galvanostatic OER electrolysis at 10 mA cm^{-2} for (a) 20 min, (b) 60 min, (c) 180 min, and (d) 600 min.

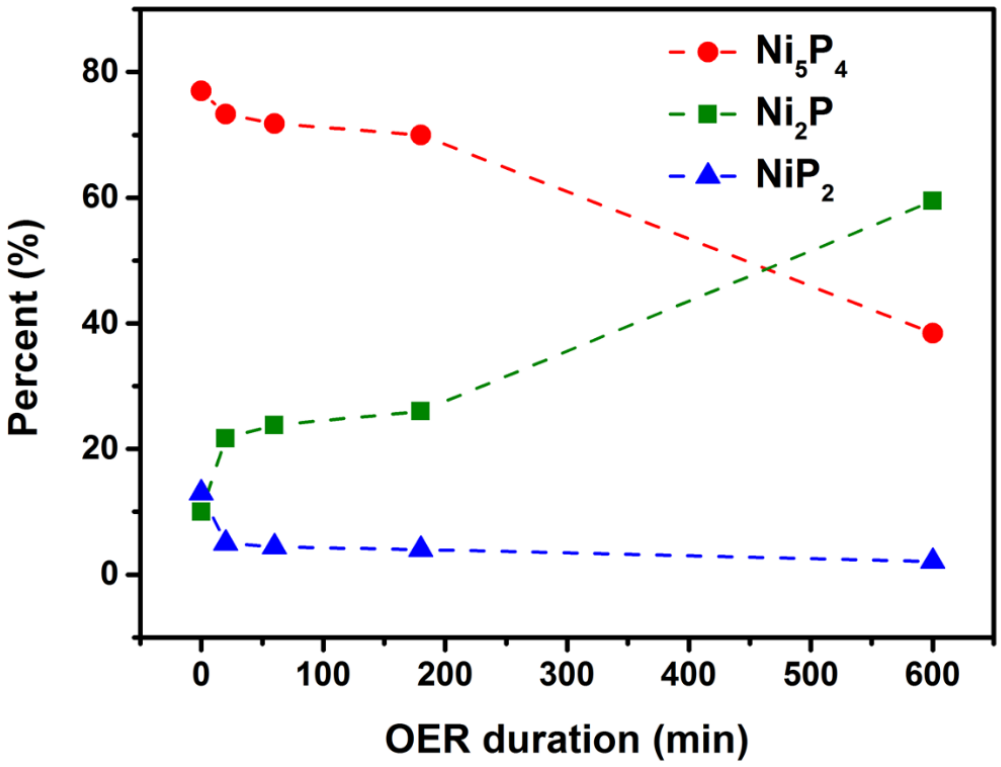

Figure S11. Variation in the percentage of different Ni-P phases with the duration of galvanostatic OER electrolysis (1.0 M KOH, 10 mA cm^{-2}).

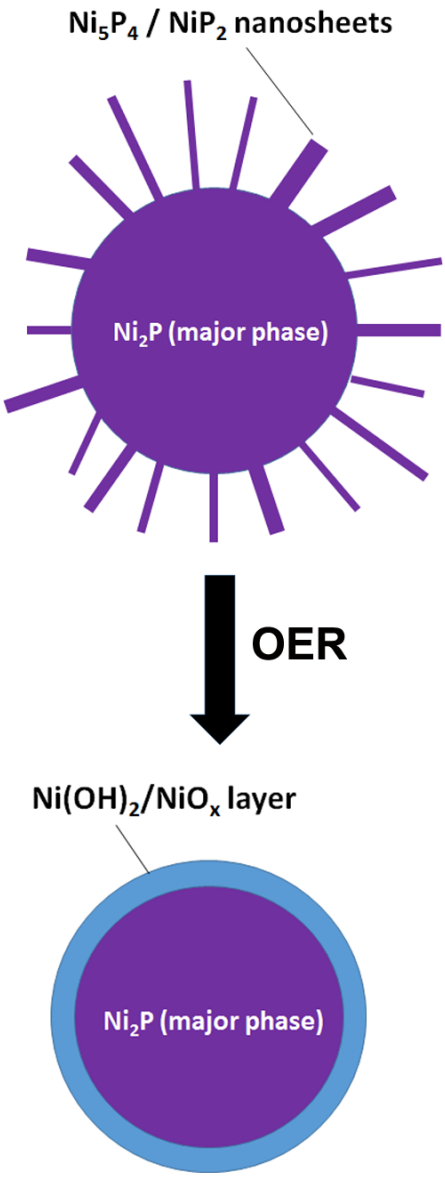

Figure S12. Schematic illustration of the structural and compositional changes taking place over the cross-section of a ligament of the porous Ni-P foam during the OER. Upon the OER, a Ni-P/ NiO ($Ni(OH)_2$) heterojunction is formed with the first few micrometers beneath the ligament surface consisting of Ni and O, and the underneath "core" consisting mainly of Ni and P. This is consistent with the previous report.[S4]

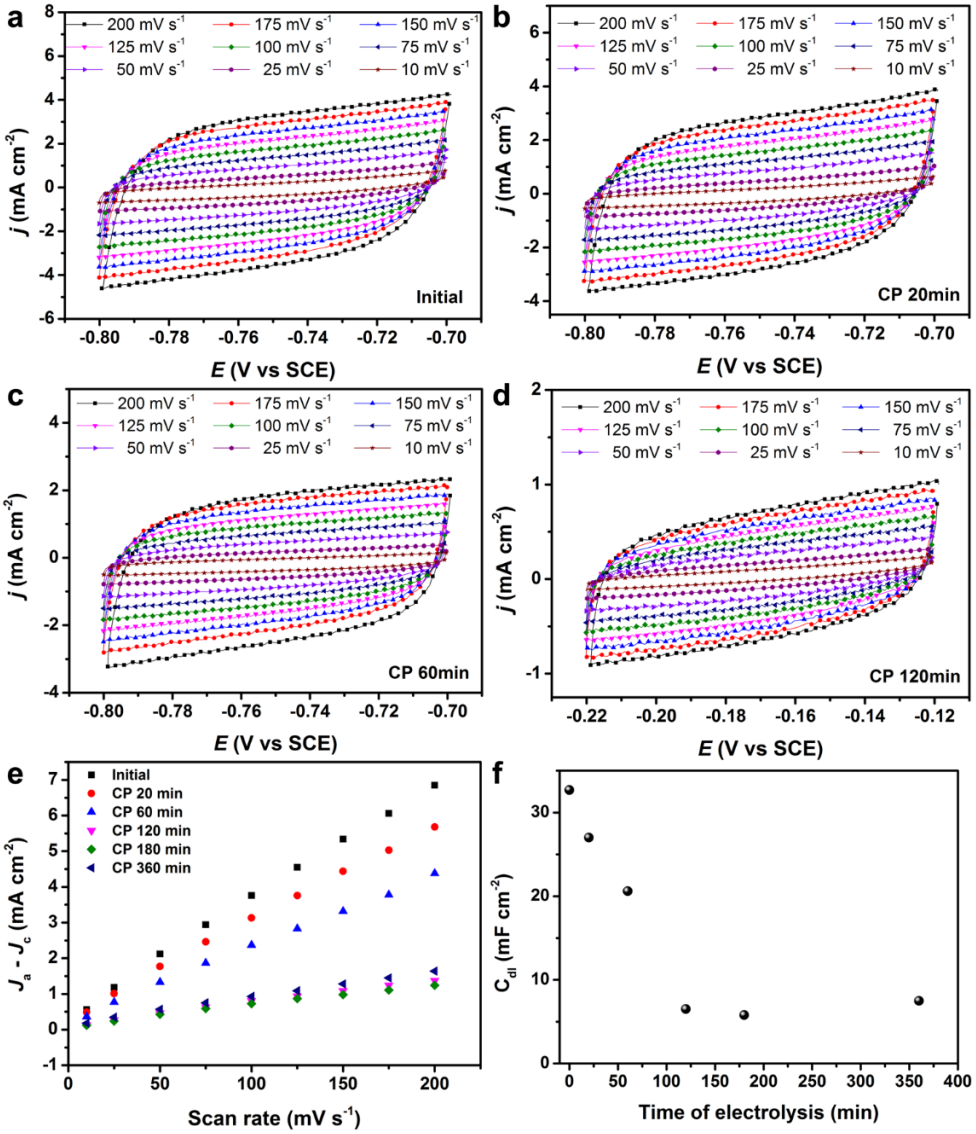

Figure S13. Cyclic voltammograms showing the capacitive behaviors of electrochemical double-layers of the porous Ni-P foam electrodes subjected to galvanostatic OER electrolysis for (a) 0 min, (b) 20 min, (c) 60 min, and (d) 120 min. (e) $|J_a\text{-}J_c|$ as a function of scan rate. J_a and J_c are the anodic and cathodic current densities, respectively, at the middle of the potential window. (f) Electrochemical double layer capacitance (C_{dl}) as a function of the duration of OER electrolysis. C_{dl} decreases with the increasing electrolysis duration, suggesting that the electrochemically accessible surface area reduces over time.

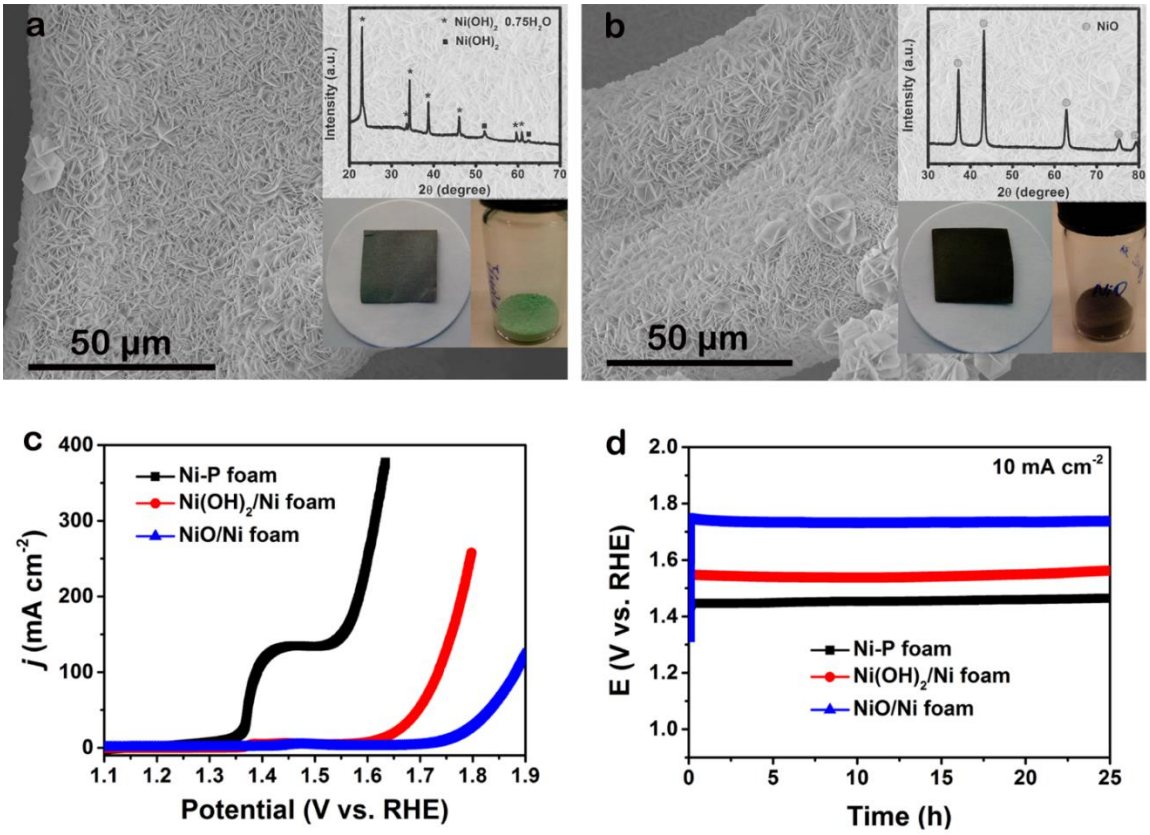

Figure S14. Morphology, structure, and electrocatalytic performance of $Ni(OH)_2$ and NiO NSs hydrothermally grown on 3D Ni foam. (a) $Ni(OH)_2$ NSs/Ni foam, (b) NiO NSs/Ni foam. The insets show digital photographs of the self-supported $Ni(OH)_2$/Ni foam and NiO/Ni foam electrodes (bottom left), $Ni(OH)_2$ and NiO NS powders (bottom right), and the corresponding XRD patterns (top). (c) Polarization curves of the porous Ni-P foam, $Ni(OH)_2$/Ni foam, and NiO/Ni foam. Scan rate: 5 mV s^{-1}. All curves are *iR*-corrected. (d) Chronopotentiometric curves of the porous Ni-P foam, $Ni(OH)_2$/Ni foam, and NiO/Ni foam measured at 10 mA cm^{-2}. All measurements were conducted in 1.0 M KOH solution at room temperature. The $Ni(OH)_2$/Ni foam was prepared as follows: First, cleaned Ni foam was placed vertically into a Teflon-lined stainless steel autoclave reactor. 10 mmol $NiCl_2$, 40 mmol $CO(NH_2)_2$, and 20 mmol NH_4F were dissolved in 100 ml DI water to form a homogeneous solution by magnetic stirring for 30 min. The solution was subsequently transferred into the autoclave. The autoclave was heated up to 120 °C for 8 h in an oven. After cooling down to room temperature, the as-formed $Ni(OH)_2$/Ni foam ($Ni(OH)_2$ powders) was taken out, rinsed with ethanol and DI water, and dried in a N_2 flow. The NiO/Ni foam (NiO powders) was obtained by calcination of $Ni(OH)_2$/Ni foam ($Ni(OH)_2$ powders) in a tube furnace at 500 °C for 3 h.[S5]

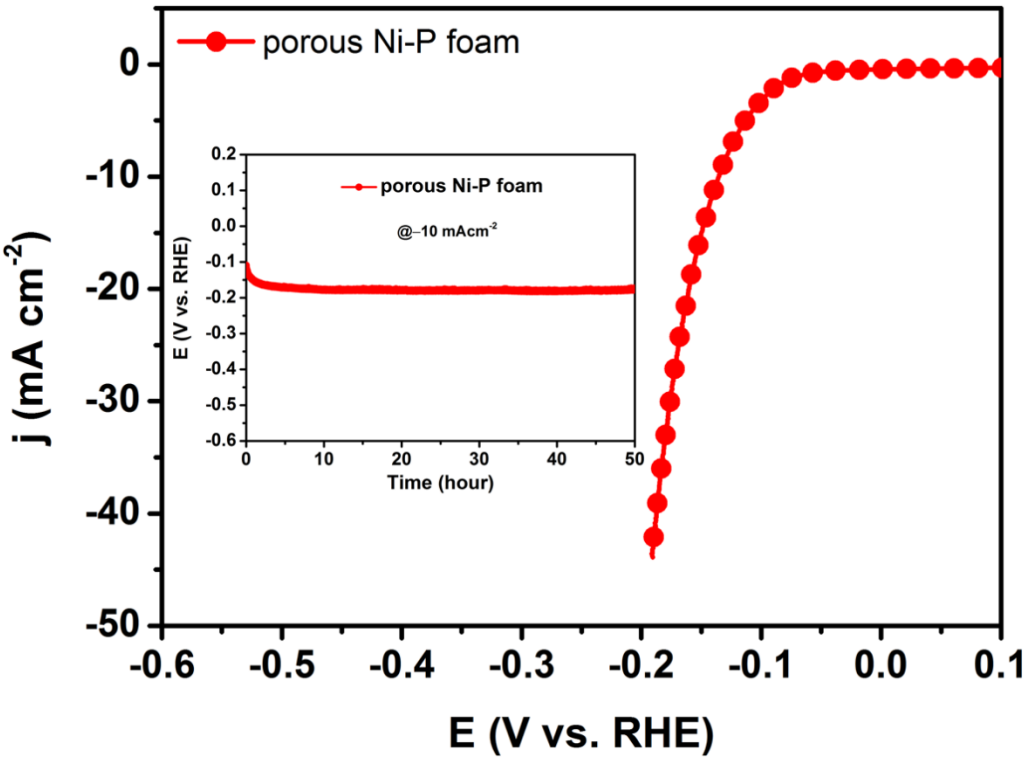

Figure S15. Polarization curve of the porous Ni-P foam electrode for HER measured in 1.0 M KOH at 5 mV s^{-1}. Inset: The durability of the electrode for galvanostatic HER electrolysis at -10 mA cm^{-2}.

Supplementary Tables:

Table S1. Comparison of the OER performance of porous Ni-P foam with that of other non-precious OER electrocatalysts reported in the literature.

OER Electrocatalyst	Electrolyte	Tafel slope (mV dec^{-1})	$j_{\eta=0.35V}$ (mA cm^{-2})	$j_{\eta=0.4V}$ (mA cm^{-2})	References
Porous Ni-P foam	1M KOH	179.9	191.0	359.6	Our Work
$Ni(OH)_2$ nanocages	1M KOH	182	1	2	*Adv. Energy Mater.* **2015**, *5*, 1401880
$Ni_2Co(OH)_x$ nanocages	1M KOH	135	2	3.5	
$NiCo(OH)_x$ nanocages	1M KOH	109	4	7.5	
$Co(OH)_2$ nanocages	1M KOH	75	4	12.5	
$NiCo_{2.7}(OH)_x$ nanocages	**1M KOH**	**65**	**10**		
Co_3O_4 NPs	0.1M KOH	59	0.4	2.5	*Adv. Mater.* **2014**, *26*, 3950-3955.
Au@Co_3O_4 NPs	0.1M KOH	60	2.8	15	
FeNC sheet/NiO	0.1M KOH	76	3	14	*Angew. Chem. Int. Ed.* **2015**, *54*, 10530-10534.
CoNC sheet/NiO	0.1M KOH	80	2	10	
Co-TiO_2	0.1 MKOH	67	0.02	0.2	*J. Phys. Chem. C* **2015**, *119*, 1921-1927.
Co-ZnO	0.1 MKOH	63	0.01	0.05	
Ni_2P NPs	1M KOH	70	2	12	*Chem. Commun.* **2015**, *51*, 11626-11629.
Ni_2P NWs	1M KOH	60	0.3	2	
Porous Co phosphide/phosphate film	1M KOH	65	~50		*Adv. Mater.* **2015**, *27*, 3175-3180.
Iron phosphide nanotube	1M KOH	43	~120		*Chem. Eur.J.***2015**, *21*,18062-8067
Ni-NiO/N-rGO Nanocomposites	0.1 MKOH	43	31		*Adv. Func. Mater.* **2015**, *25*, 5799-5808.
Co-CoO/N-rGO Nanocomposites	0.1 MKOH	56	5	11	
CoO/N-rGO	0.1 MKOH		18		

nanocomposites					
N/Co-doped PCP//NRGO	0.1 MKOH		6.5	8	*Adv. Func. Mater.* **2015**, *25*, 872-882.
N/Co-doped PCP	0.1 MKOH		2	2.5	
Co_3O_4-NRs	1M NaOH	65	2	5	*Adv. Energy Mater.* **2015**, *5*, 1500091
NCO-NRs	1M NaOH	54	10	20	
NCO-HNSs	1M NaOH	51	17	29	
N-CG-CoO Nanohybrids	1M KOH	71	12	33	*Energy Environ. Sci.* **2014**, *7*, 609-616.
CG-CoO nanohybrids	1M KOH	75	2	7	
Co_3O_4 NWs	1M NaOH	60	0.4	2.8	*Adv. Mater.* **2010**, *22*, 1926-1929.
$Ni_xCo_{3-x}O_4$ NWs	1M NaOH	64	1.3	8.9	
Co-Pi@PGF	0.1M NaOH	55.8	1	7.5	*Electrochem. Commun.* **2014**, *48*, 35-39.
Co-Pi planar film	0.1M NaOH	89.1	0.05	1	
Porous MnNi powder	0.1M KOH		2.5	6	*Adv. Func. Mater.* **2015**, *25*, 393-399.

References:

S1. Zoulias, E.; Varkaraki, E.; Lymberopoulos, N. A Review on Water Electrolysis. http://www.cres.gr/kape/publications/papers/dimosieyseis/ydrogen/A%20REVIEW%20ON%20WATER%20ELECTROLYSIS.pdf

S2. Abe, I. Energy Carriers and Conversion Systems – Vol. 1 – Alkaline Water Electrolysis, in Encyclopedia of Life Support Systems (EOLSS), Eolss Publishers, Paris, France [http://www.eolss.net/sample-chapters/c08/e3-13-03-02.pdf]

S3. H. Okamoto, Ni-P (Nickel-Phosphorus), *J. Phase Equilib.* **2000**, *21*, 210.

S4. Ledendecker, M.; Calderon, S. K.; Papp, C.; Steinruck, H. P.; Antonietti, M.; Shalom, M. The Synthesis of Nanostructured Ni_5P_4 Films and their Use as a Non-Noble Bifunctional Electrocatalyst for Full Water Splitting. *Angew. Chem. Int. Ed.* **2015**, *127*, 12538-12542.

S5. H. Long, T. L. Shi, H. Hu, S. L. Jiang, S. Xi, Z. R. Tang, Growth of Hierarchal Mesoporous NiO Nanosheets on Carbon Cloth as Binder-free Anodes for High-performance Flexible Lithium-ion Batteries. *Sci. Rep.* **2014**, *4*, 7413.